

# THE EXTENDED QUARK SIGMA MODEL AT FINITE TEMPERATURE AND BARYONIC CHEMICAL POTENTIAL

*M. Abu-Shady*<sup>a,b</sup>, *M. Soleiman*<sup>a,c</sup>

<sup>a</sup>Joint Institute for Nuclear Research, Dubna

<sup>b</sup>Department of Mathematics, Faculty of Science, Menoufia University, Egypt

<sup>c</sup>Department of Physics, Faculty of Science, Cairo University, Egypt

An extended quark sigma model which includes higher-order mesonic interactions is studied at the finite baryonic chemical potential  $u_B$  and temperature  $T$ . The field equations have been solved in the mean-field approximation by using the modified iteration method at finite baryonic chemical potential  $u_B$  and temperature  $T$ . The Goldstone theorem is satisfied below a critical temperature in the chiral limit for  $u_B = 0$ . As expected from general universality, the chiral phase transition is second-order. By including the higher-order mesonic interactions, the critical temperature is reduced compared to that found in recent works and is in good agreement with lattice QCD results. The nucleon mass is examined in the  $(u_B, T)$  plane, showing a strong dependence on  $u_B$  and  $T$ . We find that an increase in both the baryonic chemical potential  $u_B$  and the temperature  $T$  leads to an increase in the values of the nucleon mass. This is evidence for the quark–gluon deconfinement phase transition at higher values of temperature.

Представлена расширенная кварковая сигма-модель, включающая взаимодействия мезонов высших порядков. Модель рассматривается с конечными барионным химическим потенциалом  $u_B$  и температурой  $T$ . Полевые уравнения решаются в приближении среднего поля с помощью модифицированного метода итераций для конечных барионного химического потенциала  $u_B$  и температуры  $T$ . Теорема Голдстоуна выполняется ниже критической температуры в киральном пределе для  $u_B = 0$ . В соответствии с ожиданиями общей универсальности киральный фазовый переход выполняется во втором порядке. При учете мезонных взаимодействий высших порядков величина критической температуры снижается по сравнению с величинами, полученными в недавно опубликованных работах, и находится в хорошем согласии с результатами решеточной КХД. Масса нуклона рассматривается в плоскости  $(u_B, T)$  и демонстрирует сильную зависимость от  $u_B$  и  $T$ . Показано, что одновременное увеличение потенциала и температуры приводит к увеличению массы нуклона, что является проявлением кварк-глюонного фазового перехода деконфайнмента при высоких температурах.

PACS: 11.10.Wx; 11.30.Rd; 12.39.Fe

## INTRODUCTION

The behavior of quantum chromodynamics (QCD) at high temperatures and densities has received much attention over the past years and is an ongoing topic of both theoretical and experimental research [1]. Understanding the behavior of strongly interacting matter at finite temperature and/or density is of fundamental interest and has important applications

in cosmology, the astrophysics of neutron stars, and the physics of relativistic heavy-ion collisions. In fact, lattice simulations, which work well for zero baryon chemical potential and finite temperature, have serious difficulties in dealing with the complex fermion determinant that arises at finite chemical potential [2]. Different models have been used to study this problem. One of the effective models for describing the strong-interaction properties is the linear sigma model, which was suggested by Gell-Mann and Levy [3] to describe nucleons interacting via sigma ( $\sigma$ ) and pion ( $\pi$ ) exchanges. The linear sigma model clarifies how the structure of the nucleon respects the constraints imposed by chiral symmetry. Spontaneous and explicit chiral symmetry breaking require the existence of the pion mass. Furthermore, the model and its extension provides a good description of the hadron properties at zero temperature as explained in [4, 5]. At finite temperature, the model provides a good description of the phase transition by using the Hartree approximation [6–9] within the Cornwall–Jackiw–Tomboulis (CJT) formalism [10]. The model has been extended to include the finite chemical potential and finite temperature using different techniques as in [11–13] to study the phase transition and critical point. At the same time, the phase transition has been studied in the form of a mixed phase of physical vacuum and baryon matter in the framework of the Nambu–Jona-Lasinio (NJL) model as in [14, 15].

In recent years, higher-order multi-quark interactions have played an important role in studying the phase transition and critical temperature in the chiral quark models. Osipov et al. [16] studied the effect of eight-quark interactions on the critical temperature by combining the three-flavor Nambu–Jona-Lasinio model and 't Hooft Lagrangians (NJLH). Kashiwa et al. [17] extended the (NJL) model to eight-quark interactions and studied the effect of these interactions on the critical temperature point and the phase transition. Hiller et al. [18] studied the phase diagram for the (NJL) model with 't Hooft and eight-quark interactions. In the same direction, Abu-Shady studied the effect of eight higher-order mesonic interactions on nucleon properties at finite temperature [19].

The aim of this work is to study the effect of the eight higher-order mesonic interactions on the meson masses, the phase transition, the critical point temperature, and the nucleon mass at finite chemical potential and temperature in the chiral quark sigma model for small quark mass.

This paper is organized as follows: the linear sigma model with the effective mesonic potential at finite temperature is presented in Sec. 1. Next, the numerical calculations are presented in Sec. 2 and the results are discussed in Sec. 3. Finally, the summary and conclusion are presented in Sec. 4.

## 1. THE CHIRAL QUARK SIGMA MODEL WITH THE EFFECTIVE POTENTIAL

**1.1. The Chiral Quark Sigma Model with the Effective Normal Mesonic Potential.** The interactions of the quarks via  $\sigma$  and  $\pi$  meson can be described at finite temperature  $T$  and baryonic potential  $u_B$  [20]. The Lagrangian density is

$$L(r) = i\bar{\Psi}\partial_\mu\gamma^\mu\Psi + \frac{1}{2}(\partial_\mu\sigma\partial^\mu\sigma + \partial_\mu\pi\cdot\partial^\mu\pi) + g\bar{\Psi}(\sigma + i\gamma_5\boldsymbol{\tau}\cdot\boldsymbol{\pi})\Psi - U_1^{\text{eff}}(\sigma, \boldsymbol{\pi}, T, u_B), \quad (1)$$

where

$$U_1^{\text{eff}}(\sigma, \boldsymbol{\pi}, T, u_B) = U_1^{(0)}(\sigma, \boldsymbol{\pi}) - 12 \int \frac{d^3P}{(2\pi)^3} \left[ \sqrt{P^2 + M^2} + T \ln \left( \exp \left( \frac{u_B}{T} - \frac{1}{T} \sqrt{P^2 + M^2} \right) + 1 \right) + T \ln \left( \exp \left( -\frac{u_B}{T} - \frac{1}{T} \sqrt{P^2 + M^2} \right) + 1 \right) \right], \quad (2)$$

with

$$U_1^{(0)}(\sigma, \boldsymbol{\pi}) = \frac{\lambda^2}{4} (\sigma^2 + \boldsymbol{\pi}^2 - \nu^2)^2 + m_\pi^2 f_\pi \sigma. \quad (3)$$

In Eq. (2), the first term  $U_1^{(0)}(\sigma, \boldsymbol{\pi})$  is the contribution from the mesons at tree level. The divergent second term comes from the negative energy states  $\{E = \sqrt{P^2 + M^2}\}$  of the Dirac sea. It can be partly absorbed in the coupling constant  $\lambda^2$  and the constant  $\nu^2$  by using a renormalization procedure [20]. In the mean-field approximation, the meson fields are treated as time-independent classical fields. This means that we replace the powers and the products of the meson fields by their corresponding powers and the products of their expectation values. So the constituent quark mass is defined as  $M^2 = g^2 (\sigma^2 + \boldsymbol{\pi}^2)$ . The meson-meson interactions in Eq. (3) lead to a hidden chiral  $SU(2) \times SU(2)$  symmetry assuming a vacuum expectation value of

$$\langle \sigma \rangle = f_\pi, \quad (4)$$

where  $f_\pi = 93$  MeV is the pion decay constant. The final term in Eq. (3) is included to break the chiral symmetry explicitly. It leads to a partial conservation of axial-vector isospin current (PCAC). The parameters  $\lambda^2$  and  $\nu^2$  can be expressed in terms of  $f_\pi$  and the masses of mesons as follows:

$$\lambda^2 = \frac{m_\sigma^2 - m_\pi^2}{2f_\pi^2}, \quad (5)$$

$$\nu^2 = f_\pi^2 - \frac{m_\pi^2}{\lambda^2}. \quad (6)$$

**1.2. The Effective Mesonic Potential with Higher-Order Mesonic Interactions.** In this subsection, we construct the effective potential with higher-order mesonic interactions in the linear sigma model. To include higher-order mesonic interactions, we take the meson potential  $U_2^{T(0)}$  at zero temperature in the same form as in [21]:

$$U_2^{T(0)}(\sigma, \boldsymbol{\pi}) = \frac{\lambda_1^2}{4} (\sigma^2 + \boldsymbol{\pi}^2 - \nu_1^2)^2 + \frac{\lambda_2^2}{4} \left( (\sigma^2 + \boldsymbol{\pi}^2)^2 - \nu_2^2 \right)^2 + m_\pi^2 f_\pi \sigma. \quad (7)$$

Applying the minimizing conditions and the PCAC, we get

$$\lambda_1^2 = \frac{m_\sigma^2 - m_\pi^2}{4f_\pi^2}, \quad \nu_1^2 = f_\pi^2 - \frac{m_\pi^2}{\lambda_1^2} \quad (8)$$

and

$$\lambda_2^2 = \frac{m_\sigma^2 - 3m_\pi^2}{16f_\pi^6}, \quad \nu_2^2 = f_\pi^4 - \frac{m_\pi^2}{2\lambda_2^2 f_\pi^2}. \quad (9)$$

So we rewrite the effective potential in the higher-order mesonic interactions as follows:

$$U_2^{\text{eff}}(\sigma, \boldsymbol{\pi}, T, u_B) = U_2^{(0)}(\sigma, \boldsymbol{\pi}) - 12 \int \frac{d^3p}{(2\pi)^3} \left[ \sqrt{P^2 + M^2} + T \ln \left( \exp \left( \frac{u_B}{T} - \frac{1}{T} \sqrt{P^2 + M^2} \right) + 1 \right) + T \ln \left( \exp \left( -\frac{u_B}{T} - \frac{1}{T} \sqrt{P^2 + M^2} \right) + 1 \right) \right]. \quad (10)$$

We expand the effective potential in the powers of  $M^2$  which ensures that the potential satisfies the chiral symmetry when  $m_\pi \rightarrow 0$  [20]. We obtain

$$U_2^{\text{eff}}(\sigma, \boldsymbol{\pi}, T, u_B) = U_2^{T(0)}(\sigma, \boldsymbol{\pi}) - \frac{6}{\pi^2} \left( \frac{7\pi^4}{180} T^4 + \frac{\pi^2}{6} T^2 u_B^2 + \frac{1}{12} u_B^4 \right) + 6g^2 \left( \frac{T^2}{12} + \frac{u_B^2}{4\pi^2} \right) (\sigma^2 + \boldsymbol{\pi}^2). \quad (11)$$

This technique is successfully used to predict the phase transition and critical temperature as in [22]. Hence, this technique is suitable for studying the confinement and deconfinement phases in the  $(T, \mu_B)$  plane. The finite temperature vacuum can be defined by minimizing the effective potential as

$$\left. \frac{\partial U_2^{\text{eff}}(\sigma, \boldsymbol{\pi}, T, u_B)}{\partial \sigma} \right|_{\sigma=\sigma_0, \boldsymbol{\pi}=0} = 0. \quad (12)$$

Equation (12) represents the condition necessary to satisfy the spontaneous breaking of chiral symmetry, thereby satisfying the Goldstone theorem, where  $\sigma_0(T, u_B) = f_\pi(1 + \delta(T, u_B))$ . Using Eqs. (11) and (12), we obtain

$$\lambda_1^2 (\sigma_0^2 - \nu_1^2) \sigma_0 + 2\lambda_2^2 (\sigma_0^4 - \nu_2^2) \sigma_0^3 + m_\pi^2 f_\pi + 12g^2 \left( \frac{T^2}{12} + \frac{u_B^2}{4\pi^2} \right) \sigma_0 = 0. \quad (13)$$

In the chiral limit ( $m_\pi = 0$ ), Eq. (13) takes the form

$$\left[ \frac{m_\sigma^2}{4f_\pi^2} (\sigma_0^2 - f_\pi^2) + \frac{m_\sigma^2}{8f_\pi^6} (\sigma_0^4 - f_\pi^4) \sigma_0^2 + 12g^2 \left( \frac{T^2}{12} + \frac{u_B^2}{4\pi^2} \right) \right] \sigma_0 = 0. \quad (14)$$

The square of the sigma mass is obtained as the second derivative of the effective potential as in [23, 24]:

$$M_\sigma^2 = \left. \frac{\partial^2 U_2^{\text{eff}}(\sigma, \boldsymbol{\pi}, T, u_B)}{\partial \sigma^2} \right|_{\sigma=\sigma_0, \boldsymbol{\pi}=0}, \quad (15)$$

$$M_\sigma^2 = \lambda_1^2 (3\sigma_0^2 - \nu_1^2) + 2\lambda_2^2 (7\sigma_0^6 - 3\nu_2^2 \sigma_0^2) + 12g^2 \left( \frac{T^2}{12} + \frac{u_B^2}{4\pi^2} \right).$$

Similarly,

$$M_\pi^2 = \left. \frac{\partial^2 U_2^{\text{eff}}(\sigma, \boldsymbol{\pi}, T, u_B)}{\partial \pi^2} \right|_{\sigma=\sigma_0, \boldsymbol{\pi}=0}, \quad (16)$$

$$M_\pi^2 = \lambda_1^2 (\sigma_0^2 - \nu_1^2) + 2\lambda_2^2 (\sigma_0^4 - \nu_2^2) \sigma_0^2 + 12g^2 \left( \frac{T^2}{12} + \frac{u_B^2}{4\pi^2} \right). \quad (17)$$

Substituting Eq. (14) into Eqs. (15) and (17) at the chiral limit, we obtain

$$M_\sigma^2(T, u_B) = \frac{m_\sigma^2 \sigma_0^2}{2f_\pi^2} \left[ 1 + \frac{1}{2f_\pi^4} (3\sigma_0^4 - f_\pi^4) \right] \quad (18)$$

and

$$M_\pi^2(T, u_B) = 0. \quad (19)$$

From Eq. (14), we obtain two cases:

1.  $\sigma_0(T, u_B) \neq 0$ . In this case, the phase of spontaneously broken chiral symmetry leads to  $M_\pi = 0$  and  $M_\sigma \neq 0$  as in Eqs. (18) and (19). Goldstone's theorem is satisfied when the expansion of temperature is taken up to the critical temperature as in [23]. This is depicted in Fig. 1.

2.  $\sigma_0(T, u_B) = 0$ . Here the phase of restored chiral symmetry is satisfied. From Eqs. (15) and (17), we obtain  $M_\pi^2 = M_\sigma^2 = -\lambda_1^2 \nu_1^2 + 12g^2 \left( \frac{T^2}{12} + \frac{u_B^2}{4\pi^2} \right)$  as in [9]. By substituting  $\sigma_0(T, u_B) = f_\pi(1 + \delta(T, u_B))$  into Eq. (13), we obtain

$$\delta(T, u_B) = \frac{\lambda_1^2 f_\pi^2 - \lambda_1^2 \nu_1^2 + 2\lambda_2^2 f_\pi^6 - 2\nu_2^2 \lambda_2^2 f_\pi^2 + m_\pi^2 + 12g^2 \left( \frac{T^2}{12} + \frac{u_B^2}{4\pi^2} \right)}{-2\lambda_1^2 f_\pi^2 - 12\lambda_2^2 f_\pi^6 + 4\nu_2^2 \lambda_2^2 f_\pi^2 + m_\pi^2}, \quad (20)$$

where the quantity  $\sigma_0(T, u_B) = f_\pi(1 + \delta(T, u_B))$  will be referred to as the chiral phase transition as in equivalent the chiral condensate [25].

## 2. NUMERICAL CALCULATIONS AND DISCUSSION

**2.1. The Meson Fields in the Effective Potential.** In this subsection, we construct the equations of motion which result from the Lagrangian density in the mean-field approximation using the so-called «hedgehog ansatz». We assume that the pion field is radially oriented in space,  $\boldsymbol{\pi}(\mathbf{r}) = \pi(r)\hat{\mathbf{r}}$ . Due to the hedgehog solution for the pion field, a spatial rotation is equivalent to a rotation of the pion field in isospin space. Thus, rotating first in isospin space and then by the same angle in r-space leaves the hedgehog field invariant. Therefore, the fields  $\sigma(r)$  and  $\boldsymbol{\pi}(\mathbf{r})$  are eigenstates of the so-called grand spin  $\mathbf{G} = \mathbf{I} + \mathbf{J}$ , where  $\mathbf{I}$  is the isospin and  $\mathbf{J}$  is the angular momentum [26]. The Lagrangian density with the effective mesonic potential is then given by

$$L(r) = i\bar{\Psi}\partial_\mu\gamma^\mu\Psi + \frac{1}{2}(\partial_\mu\sigma\partial^\mu\sigma + \partial_\mu\boldsymbol{\pi}\cdot\partial^\mu\boldsymbol{\pi}) + g\bar{\Psi}(\sigma + i\gamma_5\boldsymbol{\tau}\cdot\boldsymbol{\pi})\Psi - U_2^{\text{eff}}(\sigma, \boldsymbol{\pi}, T), \quad (21)$$

where the sigma field is expanded around  $\sigma_0(T, u_B)$ :

$$\sigma(r) = \sigma'(r) - \sigma_0(T, u_B), \quad (22)$$

where

$$\sigma_0(T, u_B) = f_\pi(1 + \delta(T, u_B)). \quad (23)$$

Substituting Eq. (22) into Eq. (21), we obtain

$$L(r) = i\bar{\Psi}\partial_\mu\gamma^\mu\Psi + \frac{1}{2}(\partial_\mu\sigma'\partial^\mu\sigma' + \partial_\mu\boldsymbol{\pi}\cdot\partial^\mu\boldsymbol{\pi}) - g\bar{\Psi}f_\pi\Psi + g\bar{\Psi}\sigma'\Psi + ig\bar{\Psi}\gamma_5\boldsymbol{\tau}\cdot\boldsymbol{\pi}\Psi - U_2^{\text{eff}}(\sigma', \boldsymbol{\pi}, T, u_B), \quad (24)$$

where the time-independent fields  $\sigma'(r)$  and  $\boldsymbol{\pi}(r)$  satisfy the Euler–Lagrange equations, and the quark wave function satisfies the Dirac eigenvalue equation. Substituting Eq. (24) into the Euler–Lagrange equation, we get

$$\begin{aligned} \square\sigma'(r) = & g\bar{\Psi}\Psi - \lambda_1^2(\sigma' - \sigma_0)((\sigma' - \sigma_0)^2 + \boldsymbol{\pi}^2 - \nu_1^2) - \\ & - 2\lambda_2^2(\sigma' - \sigma_0)((\sigma' - \sigma_0)^2 + \boldsymbol{\pi}^2)((\sigma' - \sigma_0)^2 + \boldsymbol{\pi}^2)^2 - \nu_2^2) - \\ & - 12g^2\left(\frac{T^2}{12} + \frac{u_B^2}{4\pi^2}\right)(\sigma' - \sigma_0) - m_\pi^2 f_\pi \end{aligned} \quad (25)$$

and

$$\begin{aligned} \square\boldsymbol{\pi}(r) = & ig\bar{\Psi}\gamma_5\boldsymbol{\tau}\Psi - \lambda_1^2((\sigma' - \sigma_0)^2 + \boldsymbol{\pi}^2 - \nu_1^2))\boldsymbol{\pi} - \\ & - 2\lambda_2^2\boldsymbol{\pi}((\sigma' - \sigma_0)^2 + \boldsymbol{\pi}^2)((\sigma' - \sigma_0)^2 + \boldsymbol{\pi}^2)^2 - \nu_2^2) - 12g^2\left(\frac{T^2}{12} + \frac{u_B^2}{4\pi^2}\right)\boldsymbol{\pi}, \end{aligned} \quad (26)$$

where  $\boldsymbol{\tau}$  refers to Pauli isospin matrices,  $\gamma_5 = \begin{pmatrix} 0 & 1 \\ 1 & 0 \end{pmatrix}$ . We used the hedgehog ansatz [4] where

$$\boldsymbol{\pi}(r) = \pi(r)\hat{\mathbf{r}}. \quad (27)$$

The Dirac equations for the quarks are given in [27]:

$$\frac{du}{dr} = -p(r)u + (W - m_q + S(r))w \quad (28)$$

and

$$\frac{dw}{dr} = -(W - m_q + S(r))u + \left(\frac{2}{r} - p(r)\right)w, \quad (29)$$

where  $S(r) = g\langle\sigma'\rangle$ ,  $p(r) = \langle\boldsymbol{\pi}\cdot\hat{\mathbf{r}}\rangle$ , and  $W$  are the scalar potential, the pseudoscalar potential, and the eigenvalue of the quark's spinor  $\Psi$ , respectively. Including the color degrees of freedom, one has to replace  $g\bar{\Psi}\Psi$  by  $N_c g\bar{\Psi}\Psi$ , where  $N_c = 3$  colors,  $g$  is the

coupling constant, and  $m_q$  is the quark mass. The Dirac wave functions  $\Psi(r)$  and  $\bar{\Psi}(r)$  are given by

$$\Psi(r) = \frac{1}{\sqrt{4\pi}} \begin{bmatrix} u(r) \\ iw(r) \end{bmatrix} \quad \text{and} \quad \bar{\Psi}(r) = \frac{1}{\sqrt{4\pi}} [u(r) \ iw(r)]. \quad (30)$$

The sigma, pion, and vector densities are given by

$$\rho_s = N_c g \bar{\Psi} \Psi = \frac{3g}{4\pi} (u^2 - w^2), \quad (31)$$

$$\rho_p = i N_c g \bar{\Psi} \gamma_5 \boldsymbol{\tau} \Psi = -\frac{6g}{4\pi} uw, \quad (32)$$

$$\rho_v = \frac{3g}{4\pi} (u^2 + w^2). \quad (33)$$

The boundary conditions for the asymptotes of  $\sigma(r)$  and  $\pi(r)$  as  $r \rightarrow 0$  are

$$\sigma(r) \sim \sigma_0 \quad \text{and} \quad \pi(r) \sim 0. \quad (34)$$

We solve the Dirac equations (28) and (29) using the fourth-order Rung–Kutta method. Due to the implicit nonlinearity of Eqs. (25) and (26), it is necessary to iterate the solution until self-consistency is achieved [19].

**2.2. The Nucleon Mass.** The hedgehog baryon state is made up of three quarks in identical spinor states and hence in identical color singlet states. The hedgehog baryon state  $|B\rangle$  is a linear combination of  $N$  ( $I = J = 1/2$ ) and  $\Delta$  ( $I = J = 3/2$ ) states [4]:

$$|B\rangle = \sum_{JM} (-)^{J+M} \frac{1}{\sqrt{2}(2J+1)^{1/2}} |J = I, K = -I_3\rangle, \quad (35)$$

where we define the baryon energy as

$$E |B\rangle = M_H |B\rangle, \quad (36)$$

where  $M_H$  is the arithmetic mean of  $M_N$  and  $M_\Delta$  with an experimental value of 1086 MeV at low energy. The energy density  $\varepsilon$  is given by

$$\varepsilon = \frac{\partial L}{\partial (\partial_0 \Phi_i)} \partial_0 \Phi_i - L, \quad (37)$$

where

$$\begin{aligned} \varepsilon = & -\bar{\Psi}(i\nabla \cdot \boldsymbol{\gamma} + m_q)\Psi + \frac{1}{2} (\nabla \sigma')^2 + \frac{1}{2} (\nabla \cdot \boldsymbol{\pi})^2 - \\ & - g \bar{\Psi}(i\gamma_5 \boldsymbol{\tau} \cdot \boldsymbol{\pi} + \sigma')\Psi + U_2^{\text{eff}}(\sigma', \boldsymbol{\pi}, T, u_B) - U_2^{\text{eff}}(\sigma' = 0, \boldsymbol{\pi} = 0), \end{aligned} \quad (38)$$

which includes terms for the quark,  $\sigma'$  and  $\boldsymbol{\pi}$  kinetic energy, the quark–meson interaction, and the meson–meson interaction. The kinetic energy terms can be re-expressed via the Dirac eigenvalue equation of motion:

$$(\gamma^\mu P_\mu + g(\sigma + i\gamma_5 \boldsymbol{\tau} \cdot \hat{\mathbf{r}}\pi(r)))\Psi = 0. \quad (39)$$

Hence we obtain the kinetic energy of the quark as

$$(KE)_{\text{quark}} = -(m_q - S(r)) \rho_s(r) + E \rho_v(r) + p(r) \rho_p(r). \quad (40)$$

The kinetic energy of the sigma field is

$$(KE)_{\text{sigma}} = \frac{1}{2} \sigma' \left[ g \bar{\Psi} \Psi - \frac{\partial U_2^{\text{eff}}}{\partial \sigma'} \right]. \quad (41)$$

Similarly for the pion field, we have

$$(KE)_{\text{pion}} = \frac{1}{2} \pi \left[ g \bar{\Psi} i \gamma_5 \Psi - \frac{\partial U_2^{\text{eff}}}{\partial \pi} \right]. \quad (42)$$

The meson static energy is given by

$$E_{\text{stat}} = U_2^{\text{eff}}(\sigma', \pi, T, u_B) - U_{\text{eff}}^{T(2)}(\sigma' = 0, \pi = 0, T = 0, u_B = 0). \quad (43)$$

The sigma–quark interaction energy is

$$(m_q - g\sigma') \rho_s. \quad (44)$$

The sigma–pion interaction energy is

$$-g\pi\rho_p. \quad (45)$$

Now we can write the formula for the energy calculation of the hedgehog mass:

$$M_H = \int d^3r \varepsilon(r) = N_c W + 4\pi \int_0^\infty r^2 dr \varepsilon(r). \quad (46)$$

Therefore, we can derive the mass of the nucleon mass  $M_N$  as in [28]:

$$M_N = M_H - \frac{3}{4}l, \quad (47)$$

where  $l$  is the moment of inertia, which can be expressed only in terms of the radial functions of the pion and component quark fields [28].

### 3. DISCUSSION OF THE RESULTS

We study the phase transition, the meson masses, and the nucleon mass in the quark sigma model, in which the higher-order mesonic interactions up to the eighth-order interactions are included. We study the case with two massless quark flavors (i.e.,  $N_f = 2$ ) and  $N_c = 3$ , where  $N_c$  is the number of colors. Concentrating only on the thermal effects and ignoring quantum corrections, we examine the effect of higher-order mesonic interactions on the meson masses, and phase transition, and nucleon mass below the critical point temperature. By minimizing the effective mesonic potential  $U_2^{\text{eff}}(\sigma, \pi)$ , we obtained the gap equations (Eqs. (15) and (17)). This method is used in previous works such as [23, 24]. We solved the field equations in

the mean-field approximation by using the extended iteration method described in [19]. For numerical computation, we used the model parameters at zero temperature as the initial conditions, namely, we took  $m_\sigma = 500\text{--}700$  MeV,  $f_\pi = 93$  MeV, and the coupling constant  $g$  as a free parameter.

**3.1. Meson Masses.** We start by discussing the effect of the higher-order mesonic interactions on the sigma and pion masses as seen in Figs. 1–3 at zero chemical potential. The calculated sigma and pion masses are shown in the chiral limit ( $m_\pi = 0$ ). In Fig. 1, the effective sigma and pion masses are plotted as functions of temperature in the chiral limit. The sigma and pion masses satisfy the minimization condition in Eq. (14), which leads to a pion mass of zero below the critical temperature and a sigma mass which decreases with increasing temperature, vanishing at  $T_c = 153.43$  MeV. Therefore, the Goldstone theorem is satisfied in the  $(T, \mu_B)$  plane. We conclude that the minimization condition of the symmetry of the model is necessary to satisfy the Goldstone theorem below the critical temperature at zero baryonic chemical potential. This conclusion agrees with the findings of Nemoto et al. [24], who showed that the Goldstone theorem is satisfied when the chiral symmetry is spontaneously broken. Also, Phat and Thu [13] showed that the Goldstone theorem is satisfied when the chiral symmetry is spontaneously broken in the  $(T, \mu_I)$  plane, where  $\mu_I$  is the isospin chemical potential.

It is important to examine the effect of the coupling constant  $g$  and sigma mass  $m_\sigma$  on the behavior of the effective meson mass at the zero chemical potential. In Fig. 2, the meson mass is plotted as a function of temperature for two values of sigma masses ( $m_\sigma = 500$  and  $m_\sigma = 600$  MeV). The qualitative features of the effective sigma mass are not changed by increasing the sigma mass. The change only occurs for the critical point temperature. The change of the value  $T_c = 130$  MeV to  $T_c = 153$  MeV corresponds to  $m_\sigma = 500$  MeV and  $m_\sigma = 600$  MeV. In Fig. 3, the inverse occurs by increasing the coupling constant  $g$ .

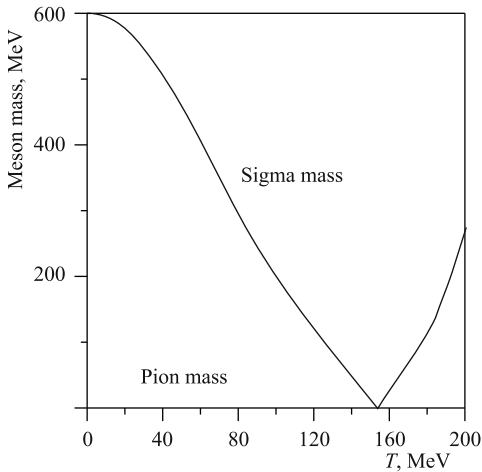


Fig. 1. The meson mass plotted as a function of temperature at zero baryonic chemical potential ( $u_B = 0$ ) in the chiral limit at  $m_\sigma = 600$  MeV and  $g = 2.26$

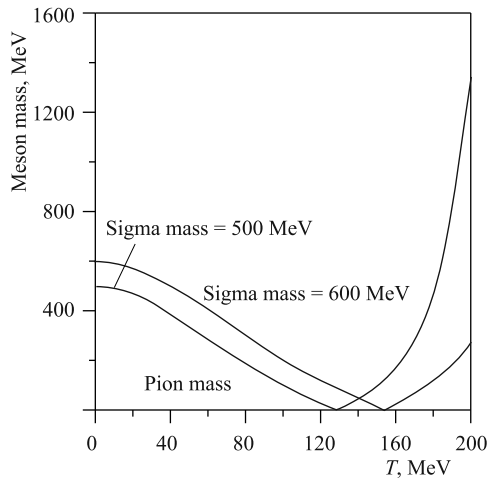


Fig. 2. The meson mass plotted as a function of temperature at zero baryonic chemical potential ( $u_B = 0$ ) in the chiral limit and for  $g = 2.26$

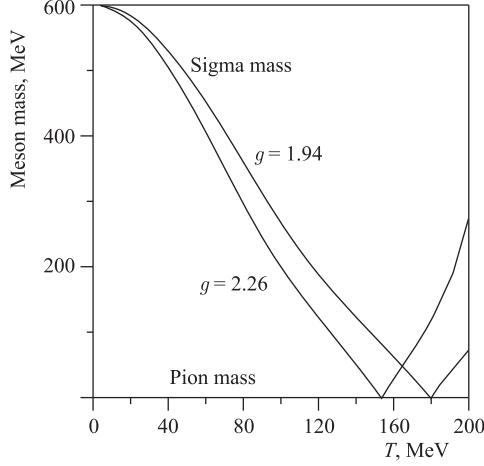


Fig. 3. The meson mass plotted as a function of temperature at zero baryonic chemical potential ( $u_B = 0$ ) in the chiral limit for two values of the coupling constant  $g$  and  $m_\sigma = 600$  MeV

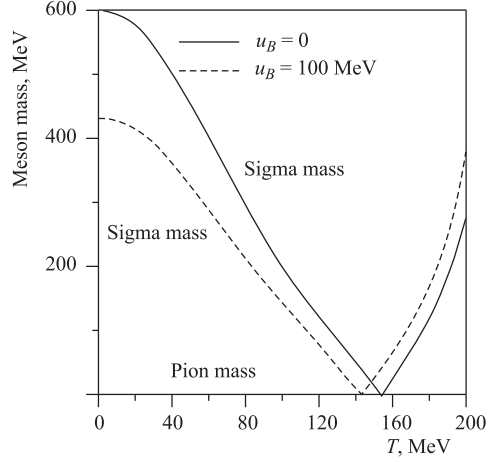


Fig. 4. The meson mass plotted as a function of temperature in the chiral limit for  $u_B = 0$ ,  $u_B = 100$  MeV at  $m_\sigma = 600$  MeV and  $g = 2.26$

The change of the value  $T_c = 153$  MeV to  $T_c = 179$  MeV corresponds to  $g = 2.26$  and  $g = 1.96$ . We know that an increase in the coupling constant increases the coupling between the meson and quark fields, which leads to the hadron becoming more bound. Therefore, we deduce that the qualitative features of the meson mass are not changed in the range parameters mentioned above. In Fig. 4, the meson mass is plotted as a function of temperature at zero baryonic chemical potential at a fixed  $u_B = 100$  MeV. The qualitative features of sigma mass are not changed by increasing the chemical potential up to  $u_B = 100$  MeV. The value of the sigma mass shifts to lower values in comparison with the behavior of sigma at zero chemical potential. In comparison with the original quark sigma model, Scanvenius et al. [20] found that the sigma mass is reduced by increasing  $u_B$  at the amount of a physical pion mass.

**3.2. The Phase Diagram.** It is important to investigate the phase transition in the  $(T, \mu_B)$  plane in the presence of higher-order mesonic interactions. At zero baryonic chemical potential, lattice QCD predicts that the phase transition is restored at about  $T_c = 151$  MeV [29]. Many attempts have been made to study the phase transition and critical point using the quark models, such as the quark sigma model, as well as the NJL model and its extensions. In Fig. 5, we plot the phase transition as a function of temperature at the zero chemical potential and finite chemical potential ( $u_B = 150$  MeV). At zero chemical potential, we note that the phase is a continuous curve and tends to zero at  $T_c = 153.43$  MeV. This indicates that the phase transition is a second-order transition. The second-order phase transition is predicted in [13,30] at zero baryonic chemical potential using the quark sigma model and the NJL model. Therefore, the higher-order mesonic interactions are not affected on the qualitative feature of the phase transition. By increasing the baryonic potential up to  $u_B = 150$  MeV, the phase transition keeps the qualitative feature of being a second-order transition. The effect only appears when the value of the critical temperature is reduced to  $T_c = 130$  MeV. We note that  $T_c = 153.43$  MeV at  $u_B = 0$ . The Wuppertal–Budapest group [29] found that

the transition temperature for the chiral restoration of  $u$ ,  $d$  quarks equals  $T_c = 151$  MeV. Hence, the present result of  $T_c$  is in good agreement with lattice QCD results. In the original quark sigma model, the critical temperature is large in comparison with lattice data at a zero chemical potential. Consequently, the higher-order mesonic interactions play an important

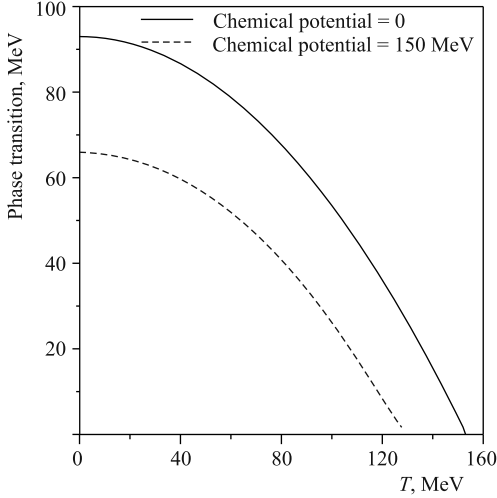


Fig. 5. The phase transition  $\sigma_0(T, u_B)$  plotted as a function of the temperature at zero chemical potential and nonzero chemical potential

role for reducing critical temperature. In comparison with the Nambu–Jona-Lasinio model with interactions of 't Hooft Lagrangians (NJLH) [16], the authors show  $T_c = 200$  MeV which is large in comparison with the lattice QCD result. By including higher-order quark interactions in the NJLH model, the critical temperature assumes a lower value, which is in agreement with lattice data. Therefore, our results indicate the same conclusion as indicated by the quark sigma model. Taniguchi and Yoshida [30] studied the chiral symmetry of QCD at finite temperature and chemical potential using the Schwinger–Dyson equation in the improved ladder approximation. They have a second-order phase transition at the temperature  $T_c = 169$  MeV along the zero chemical potential. The present results are therefore in good agreement with the results of Taniguchi and Yoshida [30] along the zero chemical potential. Kashiwa

et al. [17] studied the inclusion of the higher-order interaction term  $\sigma^4$  in the NJL model and found that the phase transition remains unchanged by including  $\sigma^4$ . In addition, they found that the NJL model, when extended to include a higher-order term of the sigma field ( $\sigma^4$ ), leads to a reduction in the critical point temperature from  $T_c = 190$  MeV to  $T_c = 180$  MeV. Therefore, our conclusion agrees with that of the NJL model.

At finite baryonic chemical potential, it is more difficult to predict the phase transition using lattice QCD due to the sign problem. Phenomenology models such as the quark sigma model and NJL model are used to describe the phase transition. The phase transition and critical point depend on the parameters of the models. In the quark sigma model, there is a first-order phase transition at zero temperature and a second-order transition at the zero chemical potential in the  $(T, \mu_B)$  plane [30]. Therefore, the critical point is found from crossing two lines of the two phases. In Fig. 6, we note that the phase transition is a continuous curve and tends to zero at  $u_B = 278$  MeV at  $T = 0$ . The phase transition has similar behavior up to  $T = 100$  MeV, indicating that the phase transition is a second-order transition for small finite temperature. Hashimoto et al. [31] found that the phase transition is a second order for zero chemical potential and small finite temperature. Moreover, the phase transition is still second-order at finite temperature at fixed  $u_B = 100$  MeV using the effective potential for the QCD-like theory. Sasaki et al. [32] studied the phase transition and a critical point using the Polyakov–Nambu–Jona-Lasinio (PNJL) model and found the phase transition does not change when a Polyakov loop in the  $(T, u_q)$  plane at a zero isospin chemi-

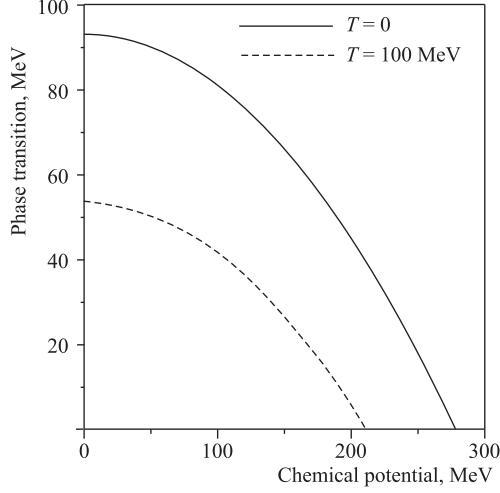


Fig. 6. The phase transition  $\sigma_0(T, u_B)$  plotted as a function of the chemical potential for zero temperature and finite temperature  $T = 100$  MeV at  $m_\sigma = 600$  MeV and  $g = 2.26$

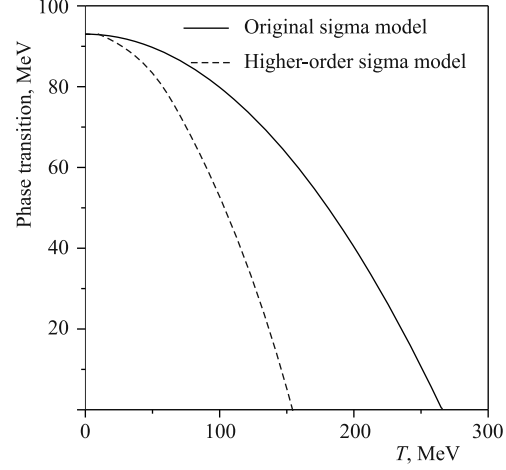


Fig. 7. The phase transition  $\sigma_0(T, u_B)$  plotted as a function of temperature for the original sigma model and the higher-order sigma model at  $u_B = 0$  and coupling constant  $g = 2.26$

cal potential is included. However, the location point moves from  $(u_q, T) = (178, 152)$  MeV to  $(u_q, T) = (187, 130)$  MeV. Moreover, the critical temperature  $T_c = 180$  MeV is large in comparison with the lattice data. Kähärä and Tuominen [12] studied the effect of the Polyakov loop on the phase diagram and critical point in the linear sigma model and the NJL model and found the critical temperature is in the range of 225–290 MeV at zero chemical potential. In Fig. 7, the phase transition  $\sigma_0(T, u_B)$  is plotted as a function of temperature for the original sigma model and the higher-order sigma model. We note that the two phases tend to zero as the continuous functions of temperature. This behavior is interpreted as a second-order phase transition. Moreover, the critical temperature is reduced to  $T_c = 153$  MeV by including the higher-order mesonic interactions up to eighth-order in the original sigma model. The obtained value  $T_c = 153$  MeV is in good agreement with lattice data [29].

**3.3. The Nucleon Mass.** In this subsection, we investigate the effect of finite temperature and baryonic potential on the nucleon mass. The nucleon mass is calculated in the mean-field approximation by using the extended iteration method as in [19]. The changes in the sigma field, pion field, and the components of the quark field under the assumptions of finite temperature and baryonic chemical potential will affect the value of the nucleon mass. Figure 8 represents the sigma field and pion field as functions of radial distance ( $r$ ) at zero temperature and chemical potential in comparison with the behavior of the sigma and pion fields at a finite temperature equal to 100 MeV and zero chemical potential. At zero temperature and chemical potential (low energy), the sigma field shows monotonic behavior. It starts at the value  $f_\pi$  and decreases with increasing radial distance  $r$  until reaching the value of  $-f_\pi$ . The pion field  $\pi(r)$  has a P-wave form with a maximum at  $r = 0.57$  fm, decreasing asymptotically, reaching a value of zero as  $r \rightarrow \infty$ . This behavior of the sigma and pion fields is in agreement [4] in the low energy limits ( $T = 0, u_B = 0$ ).

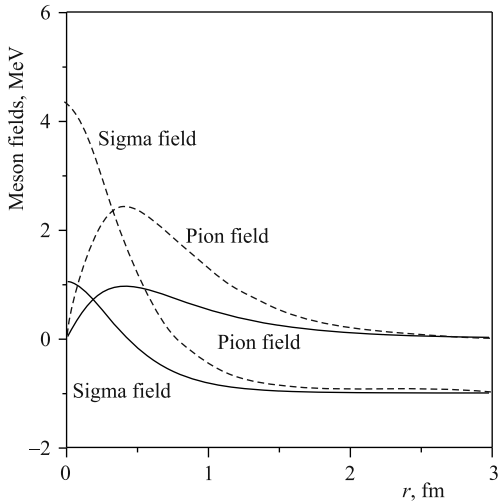


Fig. 8. The sigma and pion fields in units of  $f_\pi$  plotted as functions of distance  $r$  for  $T = 0$  and  $u_B = 0$  (solid curves) and for  $T = 100$  MeV and  $u_B = 0$  (dashed curves)

the field component  $w(r)$  shows a behavior similar to a P-wave function at zero temperature and baryonic potential. By taking  $T = 100$  MeV,  $u_B = 100$  MeV, the field component  $u(r)$  strongly increases and has a value of 0.31 at  $r = 0$  fm and decreases asymptotically to zero as  $r \rightarrow \infty$ . The finite temperature and chemical potential increase the quark contributions which will have an effect on the nucleon mass.

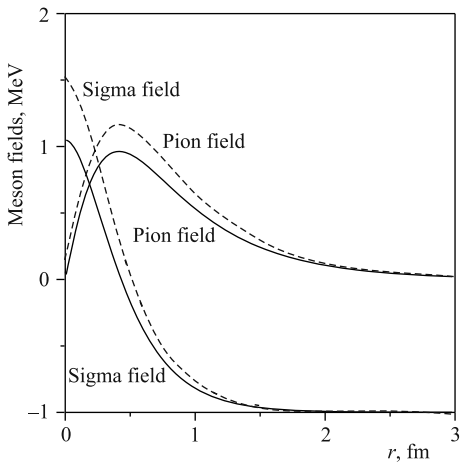


Fig. 9. The sigma and pion fields plotted as functions of distance  $r$  for  $T = 0$ ,  $u_B = 0$  (solid curves) and for  $T = 0$ ,  $u_B = 100$  MeV (dashed curves)

By including the finite temperature up to  $T = 100$  MeV in the higher-order quark sigma model, the sigma field shifts to higher values and then decreases with increasing radial distance down to  $\sigma = -f_\pi$  MeV. The pion field is shifted to higher values in comparison with the behavior at  $(T = 0, u_B = 0)$  and then it decreases with increasing radial distance. Therefore, the higher-order interactions are more affected at finite temperature. A similar situation occurs when we increase the chemical potential up to 100 MeV as in Fig.9. Thus, the value of the nucleon mass is affected by increasing mesonic contributions in the present model at finite temperature and chemical potential.

In Fig. 10, the components of the quark field ( $u(r), w(r)$ ) are plotted as functions of the radial distance  $r$ . The field component  $u(r)$  has a value of 0.06 at  $r = 0$  and decreases asymptotically to zero as  $r \rightarrow \infty$ , while the

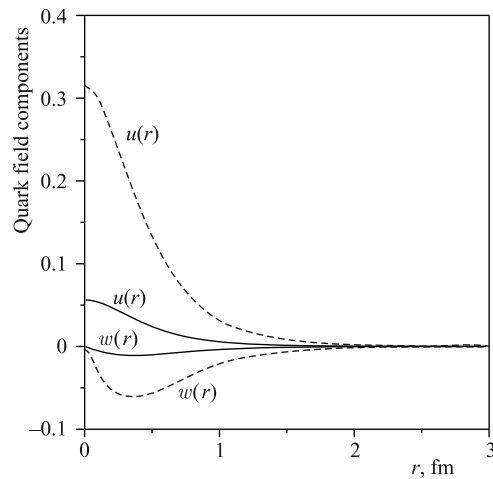


Fig. 10. The components of the quark field plotted as functions of distance  $r$  for  $T = 0$ ,  $u_B = 0$  (solid curves) and for  $T = 100$  MeV,  $u_B = 100$  MeV (dashed curves)

**The dependence of the nucleon mass on the chemical potential and temperature  
at the free parameters  $m_\sigma = 600$  MeV,  $f_\pi = 93$  MeV and  $g = 3.98$ .  
All quantities are in MeV**

Quantity	$T = 0, u_B = 0$	$T = 100, u_B = 0$	$u_B = 100, T = 100$
Quark kinetic energy	676.502	373.668	314.459
Sigma kinetic energy	271.920	56.498	109.318
Pion kinetic energy	210.64	12.716	4.928
Sigma interaction energy	285.42	309.318	455.373
Pion interaction energy	-296.105	-50.933	-26.399
Meson static energy	90.457	1910	1175.450
Baryon hedgehog mass (Eq. (46))	1238.8	2611.3	2033.129
Nucleon mass (Eq. (47))	1179	2603	2023

In the table, we investigate the effect of finite temperature and chemical potential on the dynamics of the nucleon for the smallest pion mass ( $m_\pi = 20$  MeV). We note that the meson–meson interaction energy and sigma interaction energy strongly increase at  $u_B = 0$ ,  $T = 100$  MeV which leads to an increase of the nucleon mass. A similar situation occurs when we take a baryonic chemical potential of  $u_B = 100$  MeV. Christov et al. [33] noted that the nucleon mass increases with increasing temperature up to  $(3/4)T_c$  at finite density using the linear sigma model. Dominguez and Loewe [34] calculated that the nucleon mass increases with increasing temperature. They studied the nucleon propagator at finite temperature in the framework of finite energy QCD sum rules. Abu-Shady and Mansour [35] found that the nucleon mass increases with increasing temperature using the quantized quark sigma model at finite temperature. In [34, 35], they concluded that the deconfinement phase transition is satisfied in their models at zero chemical potential.

#### 4. SUMMARY AND CONCLUSION

The chiral phase transition, the sigma and pion masses, the critical temperature, and the nucleon mass are examined in the framework of the extended linear sigma model, in which the higher-order mesonic interactions are taken into account. We calculated the sigma and pion masses by minimizing the potential. The field equations have been solved using the extended iteration method. We find that the critical temperature is reduced to lower values when the higher-order mesonic interactions are included in the linear quark sigma model. The Goldstone theorem is satisfied in the chiral limit ( $m_\pi = 0$ ) below the critical point temperature in the  $(T, u_B)$  plane. Our results suggest that the phase transition is a second-order phase transition in the chiral limit at zero chemical potential for small values of temperature up to 100 MeV. A comparison with recent model calculations is presented. The obtained results are in good agreement with lattice data. The nucleon mass is investigated in the  $(T, u_B)$  plane. We conclude that the higher-order mesonic interactions play an important role in reducing the critical temperature in the  $(T, u_B)$  plane and increasing nucleon mass.

**Acknowledgements.** The authors are grateful to Prof. A.E.Dorokhov for useful discussions which supported this work. The authors thank Profs. T.Hussien, H.El-Samman, and A.Ellithi. The authors wish to acknowledge their sponsors: the Academy of Science and Technology of Egypt and the Joint Institute for Nuclear Research in Dubna for the DIAS project. Also many thanks are to the Bogoliubov Laboratory of Theoretical Physics for the facilities provided while this work was conducted.

## REFERENCES

1. *Fischer C. S., Luecker J. // Acta Physica Polonica B. Proc. Suppl. 2012. V. 5. P. 687.*
2. *Gomez Dumm D., Scoccola N. N. // Phys. Rev. D. 2002. V. 65. P. 074021.*
3. *Gell-Mann M., Levy M. // Nuovo Cim. 1960. V. 16. P. 705.*
4. *Birse M., Banerjee M. // Phys. Rev. D. 1985. V. 31. P. 118.*
5. *Abu-Shady M., Rashdan M. // Phys. Rev. C. 2010. V. 81. P. 015203.*
6. *Petropoulos N. // J. Phys. G. 1999. V. 25. P. 2225.*
7. *Lenaghan J. T., Rischke D. H., Schaffner-Bielich J. // Phys. Rev. D. 2000. V. 62. P. 085008.*
8. *Roder D., Ruppert J., Rischke D. H. // Phys. Rev. D. 2003. V. 68. P. 016003.*
9. *Lenaghan J. T., Rischke D. H. // J. Phys. G. 2000. V. 26. P. 431.*
10. *Cornwall J. M., Jackiw R., Tomboulis E. // Phys. Rev. D. 1974. V. 10. P. 2428.*
11. *Brauner T. // Phys. Rev. D. 2006. V. 74. P. 085010.*
12. *Kähärä T., Tuominen K. // Phys. Rev. D. 2010. V. 82. P. 114026.*
13. *Phat T. H., Van Thu N. // Eur. Phys. J. C. 2011. V. 71. P. 1810.*
14. *Buballa M., Carignano S. arXiv:hep-ph/1210.7155.*
15. *Molodtsov S. V., Zinovjev G. M. // Phys. Rev. D. 2011. V. 84. P. 036011.*
16. *Osipov A. A. et al. // Phys. Lett. B. 2007. V. 646. P. 91.*
17. *Kashiwa K. et al. // Ibid. V. 647. P. 446.*
18. *Hiller B. et al. // Phys. Rev. D. 2010. V. 81. P. 116005.*
19. *Abu-Shady M. // Intern. J. Mod. Phys. E. 2012. V. 21. P. 125006.*
20. *Scanvenius O. et al. // Phys. Rev. C. 2001. V. 64. P. 045202.*
21. *Abu-Shady M. // Phys. At. Nucl. 2010. V. 73. P. 978.*
22. *Das A. Finite Temperature Field Theory. V. 6. World Scientific Publishing Co. Pte. Ltd, 1997, and references therein.*
23. *Hong C., Bo L., Huan-Qing J. // Chin. Phys. Lett. 1997. V. 14. P. 645.*
24. *Nemoto Y., Naito K., Oka M. // Eur. Phys. J. A. 2000. V. 9. P. 245.*
25. *Billic N., Nikolic H. // Eur. Phys. J. C. 1999. V. 6. P. 515.*
26. *Mosel U. Fields, Symmetries and Quarks. McGraw-Hill, 1989.*
27. *Abu-Shady M. // Intern. J. Mod. Phys. A. 2011. V. 26. P. 235.*
28. *Cohen Th.D., Broniowski W. // Phys. Rev. D. 1986. V. 34. P. 3472.*
29. *Aoki Y. et al. // Nature. 2006. V. 443. P. 675; Phys. Lett. B. 2006. V. 643. P. 46.*
30. *Taniguchi Y., Yoshida Y. // Phys. Rev. D. 1997. V. 55. P. 2283.*

31. Hashimoto Y., Tsue Y., Fujii H. arXiv:hep-ph/0506017.
32. Sasaki T. *et al.* // Phys. Rev. D. 2010. V. 82. P. 116004.
33. Christov C. V., Arriola E. R., Goeke K. // Nucl. Phys. A. 1993. V. 556. P. 641.
34. Dominguez C. A., Loewe M. // Eur. Phys. J. C. 1993. V. 58. P. 273.
35. Abu-Shady M., Mansour H. // Phys. Rev. C. 2012. V. 85. P. 055204.

Received on February 4, 2013.